

First-Order Phase Transition from the Vortex Liquid to an Amorphous Solid

M. Menghini,¹ Yanina Fasano,¹ F. de la Cruz,¹ S. S. Banerjee,² Y. Myasoedov,² E. Zeldov,² C. J. van der Beek,³
M. Konczykowski,³ and T. Tamegai^{4,5}

¹*Instituto Balseiro and Centro Atómico Bariloche, CNEA, Bariloche, 8400, Argentina*

²*Department of Condensed Matter Physics, Weizmann Institute of Science, Rehovot 76100, Israel*

³*Laboratoire des Solides Irradiés, CNRS UMR7642 and CEA-CSM-DRECAM, Ecole Polytechnique, F-91128 Palaiseau Cedex, France*

⁴*Department of Applied Physics, The University of Tokyo, Hongo, Bunkyo-ku, Tokyo 113-8656, Japan*

⁵*CREST Japan Science and Technology Corporation (JST), Tokyo, Japan*

(Received 12 October 2002; published 8 April 2003)

We present a systematic study of the topology of the vortex solid phase in superconducting $\text{Bi}_2\text{Sr}_2\text{CaCu}_2\text{O}_8$ samples with low doses of columnar defects. A new state of vortex matter imposed by the presence of geometrical contours associated with the random distribution of columns is found. The results show that the first-order liquid-solid transition in this vortex matter does not require a structural symmetry change.

DOI: 10.1103/PhysRevLett.90.147001

PACS numbers: 74.25.Qt, 74.25.Bt, 74.25.Op, 74.72.Hs

As a consequence of the interaction between vortices and quenched disorder in superconducting samples, the vortex liquid solidifies through a first-order phase transition (FOT) [1] into a topologically ordered solid with elastic deformations, the Bragg glass phase [2,3]. Correlated defects, as those produced by heavy ion irradiation, transform the first-order liquid-solid transition into a second order one in which the solid, the Bose glass [4], has no topological quasi-long-range order. However, studies [5] of the phase diagram of $\text{Bi}_2\text{Sr}_2\text{CaCu}_2\text{O}_8$ (BSCCO-2212) have shown that the FOT is robust in the presence of low density of columnar defects (CDs) even for vortex densities comparable to those of defects.

A high dose of CDs has two main effects on the vortex system. On one hand, its random distribution suppresses the FOT; on the other hand, the correlated potential hardens the vortex lines at the Bose glass transition [4]. The results in Ref. [5] indicate that the disorder induced by a low density of CDs is too weak to change the order of the liquid-solid transition. This could imply that the quasi-long-range order of the Bragg glass is preserved despite the presence of correlated defects.

The aim of this work is to establish the correlation between the spatial configuration of CDs and the vortex structure. This goal is achieved visualizing the vortex structure by means of the magnetic decoration technique in samples where the liquid-solid phase transition has been characterized by differential magneto optics (DMO) [6]. The vortex topology is discussed in terms of the nature of the liquid-solid transition.

The BSCCO-2212 samples were irradiated at GANIL by 1 GeV Pb ions parallel to the c axis of the crystal. In order to compare the vortex structure in the presence of CDs with that of the pristine sample, the irradiation was made through an *ad hoc* stainless steel mask that covers part of the samples [see inset of Fig. 1(a)]. We have investigated four samples irradiated with $B_\Phi = 5, 10, 50,$

and 100 G, where B_Φ , the matching field, is defined as $n_{\text{col}}\Phi_0$ with n_{col} the density of columns and Φ_0 the flux quantum. The H - T phase diagram obtained by DMO [7] for these samples is shown in Fig. 1(a). This

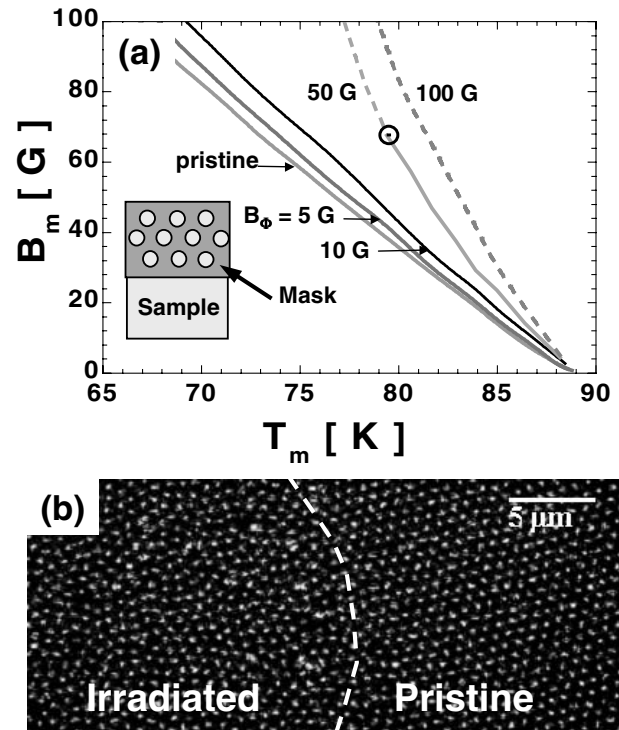


FIG. 1. (a) DMO melting lines in the H - T phase diagram for the pristine and for the $B_\Phi = 5, 10, 50,$ and 100 G BSCCO-2212 samples. Solid lines indicate first-order liquid-solid transition, while dotted lines correspond to continuous ones. Inset: Sample and mask used for irradiation. (b) Magnetic decoration at 40 G in the sample with $B_\Phi = 10$ G. The dashed line reproduces the boundary between irradiated and nonirradiated regions.

high sensitivity technique shows that the FOT is not only preserved in the presence of a low density of CDs but the transition temperature is raised when compared to that of pristine samples. For samples with $B_\Phi = 5$ and 10 G the melting line is first order, and for the $B_\Phi = 100$ G sample it is continuous in the range of fields investigated by magnetic decoration. For the $B_\Phi = 50$ G sample a critical point at 70 G separating the FOT at lower fields from a continuous one at higher fields is found. The samples containing pristine and irradiated regions were cooled in the presence of a field, FC, through the liquid-solid transition at a rate similar to that used in DMO experiments. Under this condition the structures observed in the decoration at 4.1 K correspond to that of the vortex solid.

Figure 1(b) shows the vortex structure in the nonirradiated and irradiated regions obtained by magnetic decoration after FC the $B_\Phi = 10$ G sample in a field of 40 G. A sharp boundary separates the Bragg glass in the nonirradiated region from a structure with no long range crystalline order in the irradiated one. The results show that the vortex structure in the irradiated region is polycrystalline for $B > B_\Phi$ and amorphous for $B < B_\Phi$. Examples of Delaunay triangulations of polycrystalline structures observed by FC decorations in the $B_\Phi = 10$ G sample at fields of 80 and 40 G are shown in Figs. 2(a) and 2(b), respectively. Figure 2(c) shows the vortex structure for $B = B_\Phi$. The solid dots indicate topological defects (nonsixfold coordinated vortices). Figure 3 depicts decoration images of amorphous structures obtained after FC for $B < B_\Phi$ in (a) the $B_\Phi = 50$ G sample at 30 G and (b) the $B_\Phi = 100$ G sample at 80 G.

Contrary to what is often observed in homogeneous materials, we argue that the nature of the polycrystalline structure shown in Fig. 2 is an intrinsic property. To demonstrate this we have used the dynamic annealing method [8,9] in which the magnetic field is tilted back and

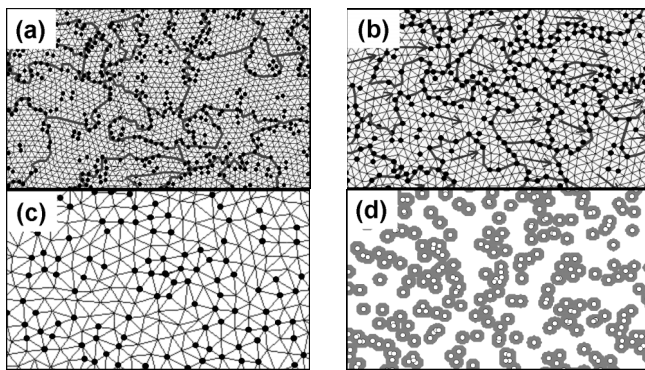


FIG. 2. Delaunay triangulations of the vortex structure in the $B_\Phi = 10$ G sample at fields of (a) 80 G, (b) 40 G, and (c) 10 G. Solid dots indicate the nonsixfold coordinated vortices. Gray lines in (a) and (b) depict grain boundaries. (d) Set of random points (white dots) simulating a distribution of CDs with $B_\Phi = 10$ G. The gray areas indicate the range of interaction of vortices localized on defects; see text. The scale bar corresponds to 10 μm .

forth before the decoration is made. This procedure is known to remove the grain boundaries in NbSe_2 and to reorder the crystalline vortex lattice [8] in nonirradiated BSCCO-2212 samples. The reordering is a result of the interaction between pancakes and Josephson vortices induced by the in-plane component of the tilted field that pin the pancake vortex lattice [10]. From the decoration results in our samples we detected that the reordering of the vortex structure was induced only in the pristine regions. The polycrystalline structure was not modified by annealing. This result supports that the polycrystalline vortex structure is an intrinsic property of the irradiated region.

The above discussion suggests that the grain boundaries are fixed in space. If this were the case, the area of the grains for a given B_Φ would be field independent contrary to what is observed in homogeneous superconductors [11]. To verify this, we studied the statistical distribution of the grain areas as a function of the applied field for $B_\Phi = 5$ and 10 G samples. The grain boundaries are defined as the interface between crystallites with orientations differing by 10° or more. The areas of the different grains are measured counting the number of vortices within them. The analysis of many pictures shows that the histogram of the grain sizes is broad with upper and lower limiting values for the grain areas for each applied field. The number of vortices, N_{vg} , within the largest and smallest grains are proportional to B as shown in Fig. 4 for the $B_\Phi = 10$ G sample. Identical behavior is found in the

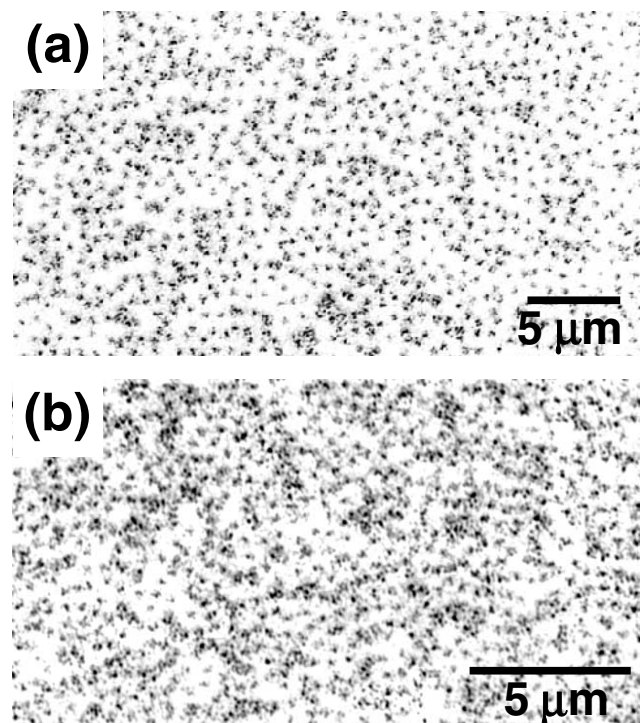


FIG. 3. Structure of the vortex solid after (a) a FOT at $B = 30$ G in the $B_\Phi = 50$ G sample and (b) a continuous liquid-solid transition at 80 G in the $B_\Phi = 100$ G sample.

$B_\Phi = 5$ G sample with the shift of the distribution of grain areas corresponding to the lower irradiation dose. Furthermore, the average number of vortices per grain (defined as the ratio between the total number of vortices within grains and the number of grains) is also proportional to B ; see Fig. 4 (solid squares). These results make evident that the size of the grains for a given B_Φ is field independent contrary to what is found in nonirradiated low T_c superconductors [11]. The invariance of the grain size with B supports that the grain size as well as its spatial distribution are determined by the landscape of CDs.

To understand the relation between grain boundaries and the distribution of correlated defects we have generated a set of random points simulating the positions of CDs; see Fig. 2(d) (white dots). This configuration is found to be equivalent to that of CDs detected after etching mica irradiated by heavy ions; see inset of Fig. 4. It is interesting to note that the distribution of CDs is not homogeneous on the scale of the lattice parameter in the range of fields investigated. The in-plane inhomogeneous distribution and the correlated character of CDs suggest the presence of a network of contours extending throughout the thickness of the sample associated with the localization of vortices on columns. In Fig. 2(d) the contours are represented by the gray connected areas indicating the range of interaction (penetration depth) of vortices localized on defects. These vortices create energy barriers that inhibit the propagation of the crystalline vortex lattice, giving rise to the polycrystalline structure in the regime $B > B_\Phi$ that has a different origin than that associated with metastable states in homogeneous systems [9]. The grain boundaries in the irradiated samples are vortex contours fixed in space by the random distribution of columns. This prompts us to propose a new state of vortex matter com-

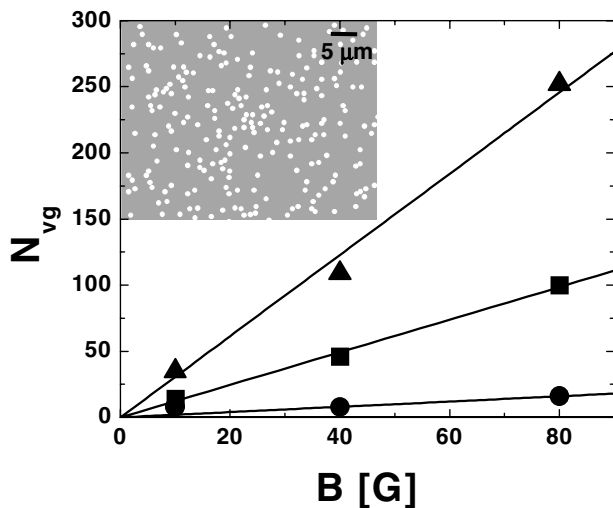


FIG. 4. Number of vortices within the largest (triangles), the average (squares), and the smallest (circles) grains as a function of B for $B_\Phi = 10$ G. Inset: Distribution of CDs in mica.

posed by two species of vortices: one corresponds to the fraction of vortices localized on contours, ρ_{cont} , and the other forms the crystallites surrounded by the contours, ρ_{crys} .

Based on the above discussion we present a picture that predicts the dependence of the number of topological defects of the polycrystalline structure, N_{def} , on B and B_Φ . The data were obtained from an area of the order of $10^4 \mu\text{m}^2$, much larger than the maximum grain size for the B_Φ investigated. We find that most of the topological defects are located along the contours separating the crystallites. Thus, as a first-order approximation we assume that N_{def} is proportional to the number of vortices on the contours, N_{cont} . The total length of the contours within the inspected area can be written as $L = N_{\text{cont}}a_0$ where a_0 is the average vortex distance. The field independence of the areas of the crystallites (see Fig. 4) implies that L is only a function of B_Φ . Therefore $N_{\text{def}} \propto N_{\text{cont}} \propto L(B_\Phi)/a_0 \propto L(B_\Phi)B^{1/2}$. The self-similarity of the random distribution of CDs imposes that the areas enclosed by the contours scale with B_Φ and consequently $L(B_\Phi) \propto B_\Phi^{1/2}$. Therefore, the fraction of vortices involved in topological defects, ρ_{def} , is

$$\rho_{\text{def}} = N_{\text{def}}/N_v \propto (B_\Phi/B)^{1/2}. \quad (1)$$

In Fig. 5 we plot ρ_{def} for all B and B_Φ investigated. The solid line corresponds to the square root dependence predicted by Eq. (1). Despite the approximations, $N_{\text{def}} \propto N_{\text{cont}}$ and $L(B_\Phi) \propto B_\Phi^{1/2}$, we see that for $B_\Phi < B$ the experimental results are well described by this simple model. The deviation of the experimental data from the dependence predicted for ρ_{def} in the range $B_\Phi/B > 1$ is evident. For $B \leq B_\Phi$ a significant fraction of the areas enclosed by the contours fixed in space are not large enough to allocate vortices with crystalline symmetry, $\rho_{\text{crys}} \approx 0$. In this limit, despite most of the vortices remaining pinned on columns, $\rho_{\text{cont}} \approx 1$, the number of

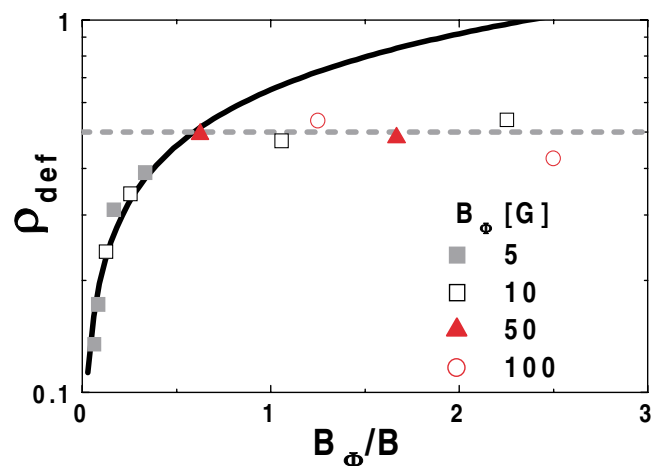


FIG. 5 (color online). Fraction of defects, ρ_{def} as a function of B_Φ/B for all B_Φ investigated. The solid line corresponds to $\rho_{\text{def}} \propto (B_\Phi/B)^{1/2}$ and the dotted line to $\rho_{\text{def}} = 0.5$.

topological defects is not proportional to $L(B_\Phi)/a_0$; i.e., a_0 is not an appropriate length scale to apply the scaling argument.

The B_Φ/B independence of the fraction of defects in the amorphous state ($\rho_{\text{def}} \approx 0.5$) is remarkable; see Fig. 5. To investigate this result we generated a random distribution of points with the constraint that the distance between nearest neighbors is not less than 50% of the lattice parameter of a lattice with the same density. This constraint allows the fluctuations of the average distance between points to be that observed in the amorphous structure. It is found that the fraction of defects obtained from Delaunay triangulation of this simulated distribution of points is the same as that for the vortex structure for $B < B_\Phi$, indicating that in this regime most of the vortices are pinned on a random distribution of CDs in agreement with experimental [12,13] and theoretical [14] results.

The analysis of the vortex structure for $B > B_\Phi$ as well as for $B < B_\Phi$, Fig. 5, strongly supports that in both limits the topological defects are associated with vortices localized on columns. For $B > B_\Phi$ the topological defects are mainly due to plastic distortions induced by the presence of crystallites. In the other limit, $B < B_\Phi$, the space within the contours does not allow the formation of crystallites, $\rho_{\text{crys}} \approx 0$, and the defects are associated with vortices localized on a fraction of columns compatible with the constraint mentioned above. It is clear that $B/B_\Phi \approx 1$ marks the transition from a topological state described by a collection of crystallites to a state characterized by an amorphous structure, both determined by the random distribution of columns.

The results discussed above show that for $B < B_\Phi$ no crystalline structure can be accommodated within the small contours determined by CDs, $\rho_{\text{crys}} \approx 0$. Thus, an amorphous vortex structure characterizes the solid state. This is particularly relevant when analyzing the interrelation between the solid structure and the nature of the vortex liquid-solid transition. The critical point at 70 G in the phase diagram of the $B_\Phi = 50$ G sample indicates that most of the field range where the first-order melting takes place corresponds to the regime $B < B_\Phi$. Thus, the observed amorphous vortex structure [see Fig. 3(a)] rules out the widely accepted correlation between a first-order liquid-solid transition and a structural symmetry transformation. Moreover, we observe no difference between the topological order in Figs. 3(a) and 3(b) despite the former structure solidifying through a FOT, whereas the latter solidifies through a continuous phase transition. It could be argued that the solid phase may have a quasi-long-range order at the melting temperature and may transform into an amorphous phase at a lower temperature. This is quite unlikely since the pancake-column interaction is effective already at the melting temperature. The FC structure becomes frozen in at temperatures lower but very close to the melting one, where a finite critical current is established [5]. The lack of field gradients in

decorated samples after FC supports that the vortex structure is not modified at length scales of the order of the lattice parameter when further cooling below the freezing-in temperature. Thus, these results pose an interesting question related to possible symmetry breaking that may occur at the first-order liquid-solid transition [15].

In summary, a new vortex matter with two species of vortices has been discovered, giving support to the suggested interstitial liquid [16] and to the vortex porous matter [7] where the boundaries of the pores are determined by the contours induced by the distribution of CDs. One specie is associated with vortices localized upon the topological contours formed by the random distribution of CDs and the other with vortices forming the crystallites. The relative distribution of vortices in these two classes explains the topological transformation of the solid from a Bragg glass ($B_\Phi = 0$) into a polycrystal ($B_\Phi < B$) and then into an amorphous structure ($B_\Phi > B$) as the density of CDs is increased. The lack of correlation between the structure of the vortex solid and the order of the melting transition opens an important question on the mechanisms that trigger melting in vortex solids. The detection of a FOT between an amorphous solid and a liquid makes evident that the first-order melting transition in vortex matter does not require the widely accepted long range structural order of the solid state.

M. M., Y. F., and F. C. acknowledge E. Jagla, P. Cornaglia, and F. Laguna for useful discussions. F. C. and E. Z. acknowledge the support by the Fundación Antorchas-WIS collaboration program. This work was partially supported by ANPCYT PICT99-5117 and by the Israel Science Foundation Center of Excellence. M. M. and Y. F. hold a scholarship of CONICET.

-
- [1] H. Safar *et al.*, Phys. Rev. Lett. **69**, 824 (1992); H. Pastoriza *et al.*, Phys. Rev. Lett. **72**, 2951 (1994); E. Zeldov *et al.*, Nature (London) **375**, 373 (1995).
 - [2] T. Giamarchi and P. Le Doussal, Phys. Rev. B **52**, 1242 (1995).
 - [3] T. Klein *et al.*, Nature (London) **413**, 404 (2001).
 - [4] D. R. Nelson and V. M. Vinokur, Phys. Rev. B **48**, 13 060 (1993).
 - [5] B. Khaykovich *et al.*, Phys. Rev. B **57**, R14 088 (1998).
 - [6] A. Soibel *et al.*, Nature (London) **406**, 282 (2000).
 - [7] S. S. Banerjee *et al.*, Phys. Rev. Lett. **90**, 087004 (2003).
 - [8] Yanina Fasano *et al.*, Phys. Rev. B **62**, 15 183 (2000).
 - [9] Yanina Fasano *et al.*, Phys. Rev. B **66**, 020512(R) (2002).
 - [10] A. E. Koshelev, Phys. Rev. Lett. **83**, 187 (1999).
 - [11] M. V. Marchevsky, Ph.D. thesis, Kamerlingh Onnes Laboratory, Leiden University, Holland, 1996.
 - [12] S. L. Lee *et al.*, Phys. Rev. Lett. **81**, 5209 (1998).
 - [13] H. Dai *et al.*, Science **265**, 1552 (1994).
 - [14] U. C. Täuber and D. R. Nelson, Phys. Rev. B **52**, 16106 (1995).
 - [15] S. Colson *et al.*, cond-mat/0204493 v2.
 - [16] L. Radzihovsky, Phys. Rev. Lett. **74**, 4923 (1995).